ACS OMEGA

http://pubs.acs.org/journal/acsodf

Article

Theoretical Study on the Atom-Substituted Quinazoline Derivatives with Faint Emission as Potential Sunscreens

Yajie Zhang, Min Ma, Changjiao Shang, Yunjian Cao, and Chaofan Sun*

Cite This: *ACS Omega* 2022, 7, 14848−14855

Read Online

ACCESS | Metrics & More | Article Recommendations | Supporting Information

ABSTRACT: Two novel compounds (HQS and HQSe) with excited-state intramolecular proton transfer (ESIPT) properties were designed based on the compound 2-(2-hydroxy-3-ethoxyphenyl)-3*H*-quinazolin-4-one (HQ). The parameters related to the ESIPT properties and electronic spectra of HQ and its derivatives were calculated using density functional theory and time-dependent density functional theory methods. The obtained geometric configurations, infrared vibrational spectra, and reduced density gradient scatter plots have shown that the intramolecular hydrogen bond $O_1\cdots H_1-N_1$ has been weakened upon photoexcitation. Moreover, from the scanned potential energy curves, it can be found that the ESIPT processes of the three compounds have no energy barriers. It is noteworthy that HQS and HQSe can strongly absorb light in the UVA region (~340 nm) and exhibit weak fluorescence emission in the visible light region, which comes from the keto configuration. The special optical properties of HQS and HQSe can promote their application as potential sunscreen agents.

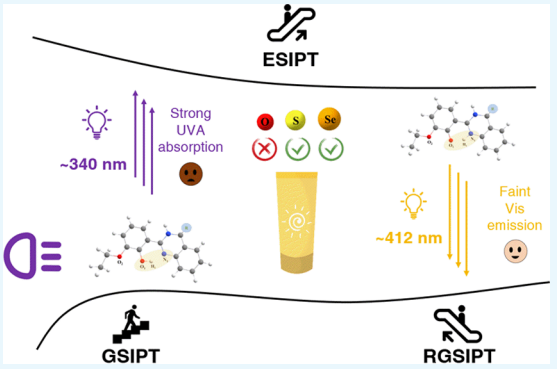

1. INTRODUCTION

Ultraviolet (UV) damage has been widely concerning because it can accelerate skin aging, cause melanin deposition, and induce skin cancer.[1−3] In general, UV rays can be classified as UVA, UVB, and UVC according to the difference in wavelength (320−400, 280−320, and 200−280 nm for UVA, UVB, and UVC, respectively),[4−6] in which UVA has intense penetration and is the most significant cause of skin aging. Therefore, the discovery, design, and synthesis of UV absorbers with special effects is significant to protecting the skin from UV damage.[7−9]

The UV absorber strongly and selectively absorbs high-energy UV rays. It then releases and consumes them with thermal energy or harmless low-energy radiation to avoid damage to the skin.[10,11] In the past few years, the applications of UV absorbers with excited-state intramolecular proton transfer (ESIPT) characteristics in sunscreen have been widely reported.[12−14] Under light excitation, compounds with ESIPT characteristics produce photoisomers through excited-state proton transfer, accompanied by double fluorescence.[15−17] Owing to their excellent application in sunscreen, they have attracted the interest of many researchers. Wu et al. reported a sunscreen molecule FPPO-HBr with ESIPT properties and found that the FPPO-HBr decays via the ESIPT process followed by the ultrafast structural distortion upon photoexcitation.[18] In addition, the ESIPT process of homosalate has been studied using time-resolved ultrafast laser spectroscopy, laser-induced fluorescence, and steady-state absorption spectroscopy methods to confirm the feasibility of homosalate as a sunscreen.[19] Moreover, the plant flavonoid compounds with ESIPT properties have been synthesized and investigated to provide a theoretical basis for sunscreen cosmetics.[20] Research on the properties of sunscreen still needs to be deeply explored.

In this work, two novel compounds, HQS and HQSe with ESIPT properties, were designed in theory by the homologous substitution (S and Se) on the synthesized molecule 2-(2-hydroxy-3-ethoxyphenyl)-3*H*-quinazolin-4-one (HQ).[21] The geometrical configurations of HQ, HQS, and HQSe in enol and keto forms are plotted in Scheme 1, and the significant atom associated with proton transfer is highlighted to aid understanding. Furthermore, the critical geometric structure parameters, infrared (IR) vibrational spectra, and RDG scatter plots of HQ, HQS, and HQSe are calculated to investigate the effect of atomic electronegativity on the intramolecular hydrogen bond (IHB). The potential energy curves (PECs) of HQ, HQS, and HQSe are calculated to study the influence of atomic substitution on the ESIPT process. It is worth noticing that the absorption and fluorescence peaks of HQS

Received: January 16, 2022
Accepted: April 12, 2022
Published: April 22, 2022

Scheme 1. Geometric Structures of HQ, HQS, and HQSe in (a) Enol and (b) Keto Forms

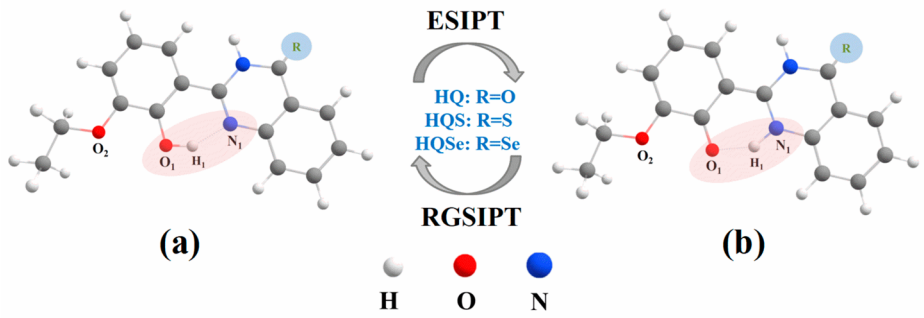

and HQSe are located in the range of UVA and visible light, respectively.

2. METHODS

In this work, the geometric structure optimizations of HQ, HQS, and HQSe in enol and keto forms at ground and excited states were calculated using density functional theory (DFT)[22−24] and time-dependent density functional theory (TD-DFT)[25−27] methods with B3LYP/6-311G(d,p),[28−30] respectively. The optimization processes of HQ and its two derivatives are shown in Figure S1. The critical hydrogen bond parameters, absorption and fluorescence spectra, IR vibrational spectra, PECs, and RDG scatter plots of HQ, HQS, and HQSe were calculated based on the optimized structures. Considering that HQ, HQS, and HQSe are endowed with an obvious charge transfer process upon photoexcitation, range-separated functional CAM-B3LYP was used to simulate the absorption and fluorescence spectra in this work.[31] Moreover, all calculations exploited the integral equation formula polarized continuum model (IEFPCM)[32,33] of THF solvent to fit the experimental data better. The PECs of HQ, HQS, and HQSe at the S_0 and the lowest excited (S_L) states were scanned by steadily increasing the bond length of O_1-H_1. The analysis of hole−electron and frontier molecular orbitals (FMOs) all use the Multiwfn 3.8 program[34] and VMD 1.9.4.[35] All calculations were performed by using Gaussian 16 software[36] in this work.

3. RESULTS AND DISCUSSION

3.1. Geometric Structure Parameters. The geometric structure parameters of HQ, HQS, and HQSe at the S_0 and S_L states were optimized by DFT and TD-DFT methods with B3LYP/6-311G(d,p), respectively. As numerous attempts to obtain the equilibrium structures of HQ and its two derivatives have culminated in failure and ended in their proton-transferred structures (HQ-k, HQS-k, and HQSe-k), herein, we only list the significant parameters associated with the IHBs of HQ-k, HQS-k, and HQSe-k, as shown in Table 1.[37] It can be found that the $O_1\cdots H_1$ bond lengths are elongated from ∼1.552 Å in the S_0 state to ∼1.689 Å in the S_L state, whereas the H_1-N_1 bond lengths are decreased from ∼1.065 Å in the S_0 state to ∼1.039 Å in the S_L state. Furthermore, all of the bond angles $\delta(O_1\cdots H_1-N_1)$ are decreased from ∼144.8° in the S_0 state to ∼141.1° in the S_L state. Generally speaking, the shorter bond length, the more planar bond angle, the more robust the IHB, the more the molecule is prone to cause the proton transfer process.[38−40] Thus, it can be concluded that the IHB $O_1\cdots H_1-N_1$ is weakened at the S_L state and verified that the reverse proton transfer (RPT) process prefers to proceed at the S_0 state.[41] Most notably, the relative ordering of the IHB intensity at S_0 and S_L states for the three investigated compounds is as follows: HQ-k < HQS-k < HQSe-k. Based on the above analysis, it can be inferred that atomic electronegativity can alter the strength of IHB in the S_0 and S_L states and thereby affect the proton transfer process of HQ.[41]

Table 1. Critical Bond Lengths (Å) and Bond Angles (deg) of HQ, HQS, and HQSe at S_0 and S_L States

	state	$O_1\cdots H_1$	H_1-N_1	$\delta(O_1\cdots H_1-N_1)$
HQ-k[a]	S_0	1.560	1.063	144.9
	S_L	1.777	1.024	138.7
HQS-k[a]	S_0	1.551	1.065	144.7
	S_L	1.702	1.040	140.6
HQSe-k[a]	S_0	1.546	1.067	144.9
	S_L	1.588	1.055	144.2

[a]The k represents the proton transfer structures of HQ and its derivatives.

3.2. Infrared Vibrational Spectra. The IR vibrational spectra of HQ, HQS, and HQSe in the keto form were obtained and are displayed in Figure 1. Apparently, the stretching vibrational mode of N_1-H_1 for HQ-k, HQS-k, and HQSe-k is separately located at 2726, 2696, and 2675 cm^{-1} in the S_0 state, which shifts to 3321, 3094, and 2823 cm^{-1} in the S_L state, implying that the IHB $O_1\cdots H_1-N_1$ is weakened upon photoexcitation and the RPT process is difficult to complete in the S_L state. It can also be noticed that the blue shifts follow the decreased order of HQ-k > HQS-k > HQSe-k, indicating that the IHB intensity has gradually weakened as the atomic electronegativity decreased, which is consistent with the analysis of the geometric parameters.[42,43]

3.3. RDG scatter plots. Reduced density gradient (RDG) is a dimensionless parameter used to describe electron heterogeneity in density functional theory. Its expression equation is[44,45]

$$\mathrm{RDG(r)} = \frac{1}{2(3\pi^2)^{1/3}}\frac{|\nabla\rho(r)|}{\rho(r)^{4/3}} \quad (1)$$

As the electron density of the molecule decays exponentially, the RDG presents a large value far away from the molecule. On the contrary, the value of RDG in the interaction region is very minimal, in which the electron density and RDG in the noncovalent interaction region are relatively low.[46] Moreover, the IRI isosurface is a useful tool for rendering an intrinsic picture of intramolecular and intermolecular hydrogen bonding.[47] Like the RDG scatter plots, it can be used to discern distinct interaction strengths and types.

The RDG scatter plots and the interaction types of HQS-k and HQSe-k at the ground and excited states are shown in

https://doi.org/10.1021/acsomega.2c00316
ACS Omega 2022, 7, 14848−14855

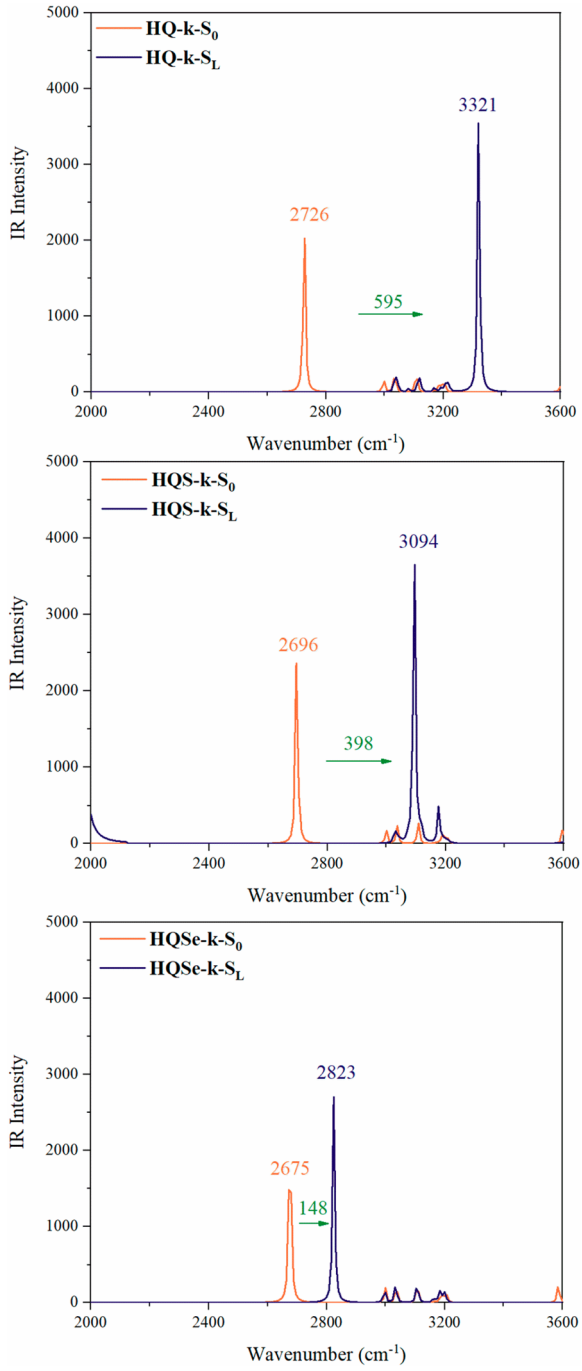

Figure 1. Simulated IR vibrational spectra in N_1-H_1 regions of HQ-k, HQS-k, and HQSe-k in the S_0 and S_L states.

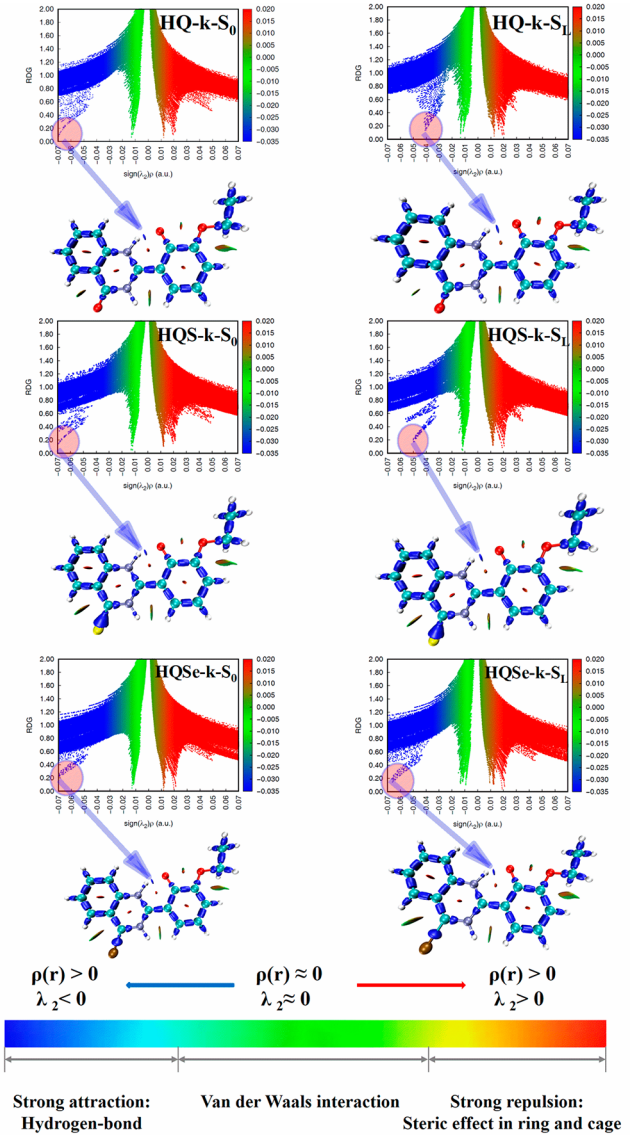

Figure 2. RDG vs sign $(\lambda_2)\rho(r)$ scatter plots and the interaction types of HQ-k, HQS-k, and HQSe-k in S_0 and S_L states.

Figure 2; it can be observed that the types of interactions of HQ-k, HQS-k, and HQSe-k at the ground and excited states are all hydrogen-bonding interactions. In RDG scatter plots, the enclosed place represents the IHB. The smaller the value here, the stronger the IHB. Obviously, for HQ-k, HQS-k, and HQSe-k, the IHB is weaker in the S_L state compared to that in the S_0 state, which is not favorable to the RPT process.[48−50] Moreover, the strengths of IHB are on the order of HQ-k < HQS-k < HQSe-k, verifying that IHBs are weakened with decreased atomic electronegativity.

3.4. Absorption and Fluorescence Spectra. The absorption and fluorescence spectra of HQ, HQS, and HQSe were calculated using the CAM-B3LYP functional based on the optimized geometric structures and plotted in Figure 3. The relevant data are shown in Table 2 and Table 3. The absorption peaks of HQ, HQS, and HQSe are situated at 277, 326, and 354 nm, respectively, in which wavelengths of HQS and HQSe are located in the range of UVA. Because HQ, HQS, and HQSe do not have stable structures in enol form in the S_L state, they do not have fluorescence spectra in enol form. Moreover, in the keto form, HQ, HQS, and HQSe emit faint fluorescence and are located at 397, 402, and 422 nm, respectively, in which wavelengths of HQS and HQSe are located in the range of visible light.[51]

As shown in Figure 3, it can be observed that the values of the absorption, fluorescence peaks, and Stokes shift of the three compounds are in the order of HQ > HQS > HQSe, indicating that atomic electronegativity can influence the optical characteristics of compounds. Moreover, it can be found that the absorption and fluorescence peaks of HQS and HQSe are located in the UVA range and the visible light range, respectively. Moreover, the oscillator strengths of fluorescence peaks are very weak, which is favorable for protecting human

https://doi.org/10.1021/acsomega.2c00316
ACS Omega 2022, 7, 14848−14855

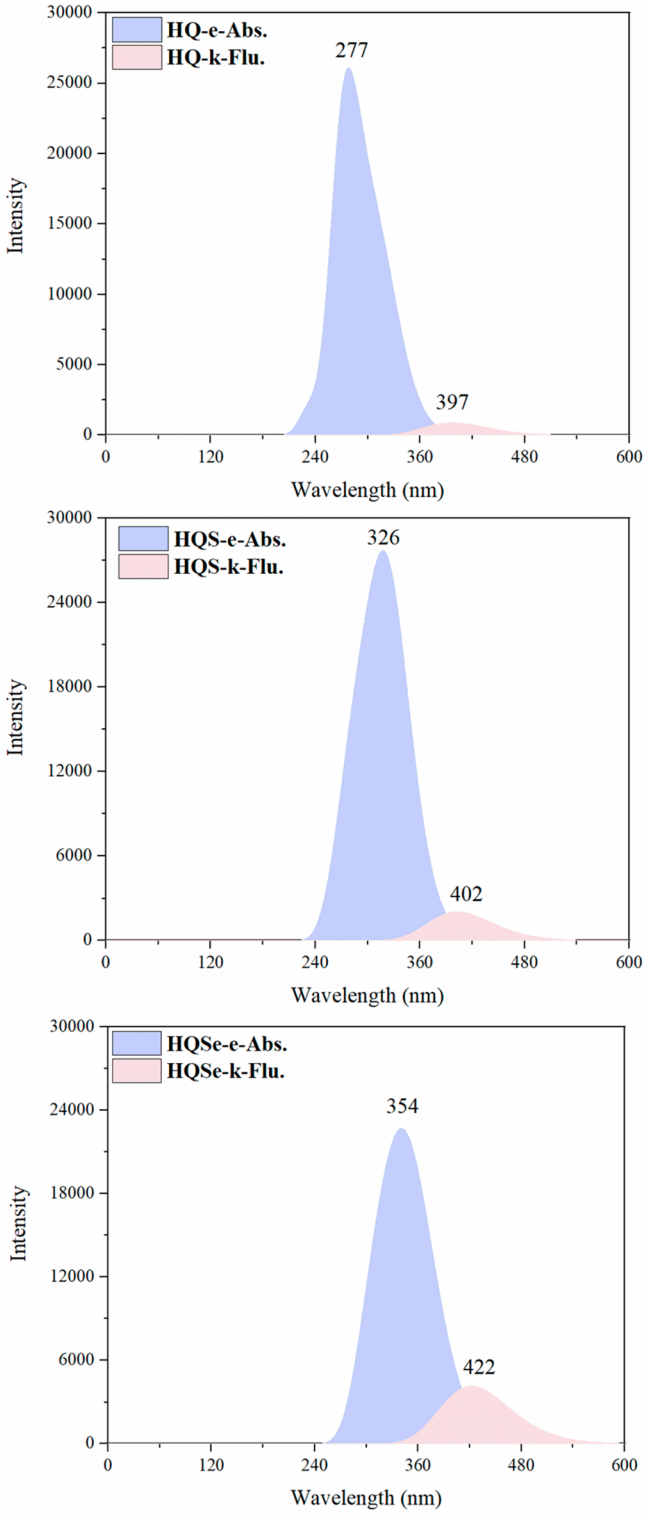

Figure 3. Absorption and fluorescence spectra of HQ, HQS, and HQSe in THF solvent.

skin. Therefore, it can be concluded that HQS and HQSe can be used as sunscreen agents.

3.5. FMO Distribution and Hole−Electron Analysis. To further explore the fundamental reason for the proton transfer process, the FMO distributions associated with the S_L state of HQ-k, HQS-k, and HQSe-k, and the corresponding energy gap values in THF were obtained and plotted in Figure 4. It can be seen that the electron density distributed on the O atom of HQ-k, HQS-k, and HQSe-k has decreased upon photoexcitation, indicating that IHB $O_1\cdots H_1-N_1$ will be weakened in the S_L state. Moreover, the corresponding energy gaps of the three investigated proton-transferred tautomers are in the following order: HQ-k (3.603 eV) > HQS-k (2.839 eV) > HQSe-k (2.758 eV), which leads to the fluorescence peak following the order: HQ-k < HQS-k < HQSe-k, illustrating that atomic electronegativity can influence the optical characteristics of the molecules.[52]

In order to determine why the fluorescence strength is weakening, the isosurface of hole−electron distribution, Cele and Chole, the overlap of hole−electron (Sr), and charge density difference (CDD) of HQ-k, HQS-k, and HQSe-k in THF solvent were obtained and plotted in Figure 5.[53−55] The quantities of transferred electrons of HQ-k, HQS-k, and HQSe-k from ethoxyphenol to quinazoline are calculated and marked in the isosurface of hole−electron distribution. It can be found that the degree of charge transfer follows HQ-k (0.934 e) > HQS-k (0.634 e) > HQSe-k (−0.020 e), and the distance between the hole and the electron can also verify this conclusion. So the fluorescence strengths are in the following order: HQ-k < HQS-k < HQSe-k. In addition, the Sr and CDD can show that HQ, HQS, and HQSe have undergone a charge transfer process,[56] which explains the fundamental reason for proton transfer.

3.6. Potential Energy Curves. To study the proton transfer process of HQ, HQS, and HQSe, the PECs of three compounds were scanned by increasing the O_1-H_1 bond length and are shown in Figure 6. In the S_0 state, the energy barriers of the forward proton transfer (FPT) process for HQ, HQS, and HQSe are 5.496, 6.443, and 6.576 kcal/mol,

Table 2. Absorption Peaks and Corresponding Transition Properties of HQ, HQS, and HQSe

	state	λ_{abs} (nm)	contribution MO	strength f
HQ-e	S_1	314	(67.434%) H→L	0.2883
	S_2	277	(59.745%) H-1→L	0.4623
	S_3	267	(46.612%) H-1→L+1	0.1534
	S_4	235	(62.840%) H-4→L+1	0.0003
	S_5	233	(51.879%) H-2→L	0.0477
	S_6	228	(64.107%) H-5→L	0.0007
HQS-e	S_1	379	(67.110%) H-2→L	0.0000
	S_2	326	(53.596%) H-1→L	0.4168
	S_3	320	(55.701%) H→L+1	0.1756
	S_4	289	(60.656%) H-1→L+1	0.2777
	S_5	277	(43.460%) H-3→L	0.0458
	S_6	263	(34.711%) H-3→L	0.0684
HQSe-e	S_1	434	(68.200%) H-2→L	0.0000
	S_2	354	(49.976%) H→L	0.3934
	S_3	323	(58.589%) H→L+1	0.2271
	S_4	302	(56.381%) H-1→L+1	0.1221
	S_5	291	(45.846%) H-3→L	0.0013
	S_6	281	(68.989%) H-2→L+1	0.0001

Table 3. Fluorescence Characteristics of HQ, HQS, and HQSe in the Keto Form in THF Solvent

	state	λ_{flu} (nm)	contribution MO	strength f
HQ-k	S_L	397	(66.838%) H→L	0.0219
HQS-k	S_L	402	(48.598%) H→L	0.0509
HQSe-k	S_L	422	(65.888%) H→L	0.1032

https://doi.org/10.1021/acsomega.2c00316
ACS Omega 2022, 7, 14848−14855

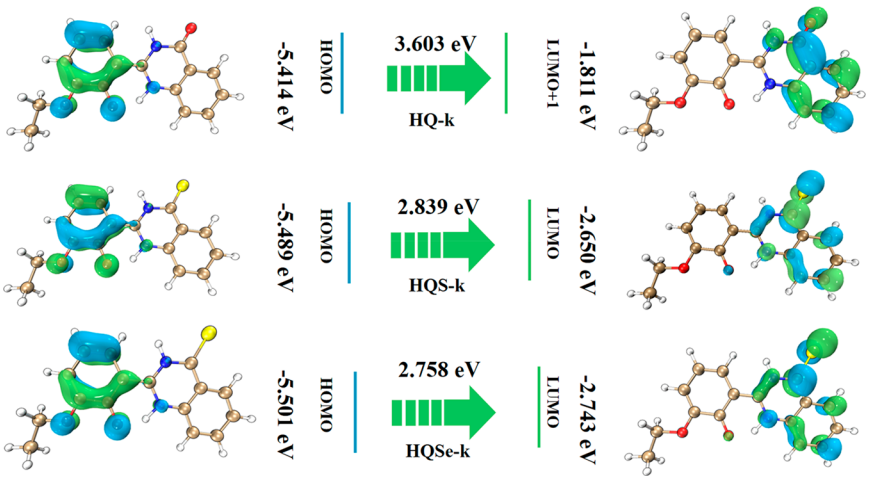

Figure 4. Frontier molecular orbital distribution and the corresponding energy gap values of HQ-k, HQS-k, and HQSe-k in THF solvent.

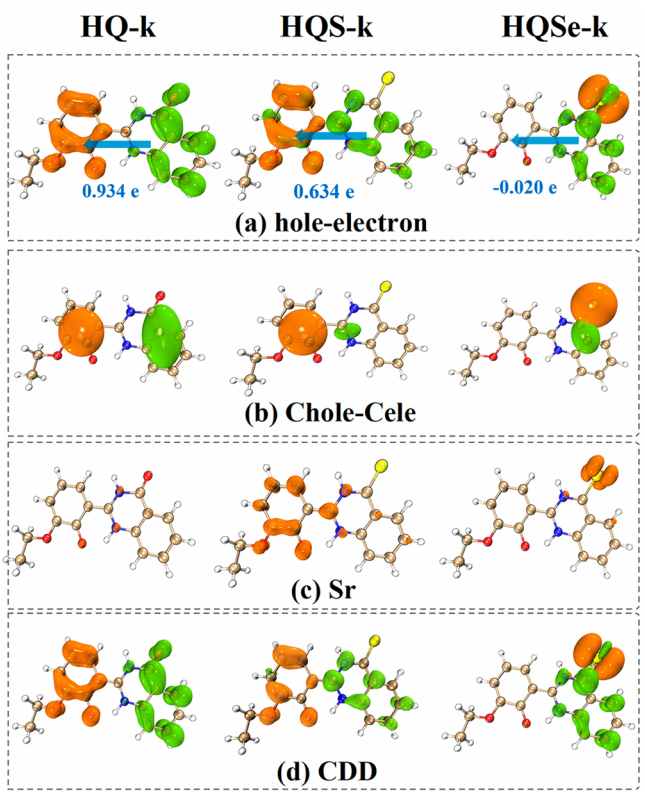

Figure 5. Isosurfaces of hole−electron distribution (a), Cele and Chole functions (b), overlap of hole−electron (Sr) (c), and charge density difference (d) of HQ, HQS, and HQSe in THF solvent. (a−c) Green represents holes and the orange represents electrons. (d) Green and orange correspond to the decrease and increase of the excited-state density relative to the ground state density, respectively.

respectively. Interestingly, we noticed that the FPT behavior has become an ultrafast process with no energy barriers in the S_L state, which explains why the three molecules do not have a stable enol form in the S_L state, and this result is consistent with the analysis of geometric structures.[57−59] For the RPT process, the negligible energy barriers (0.367, 0.194, and 0.178 kcal/mol) of HQ, HQS, and HQSe need to be surmounted in the S_0 state, while the energy continues to rise in the S_L state, implying that the RPT process prefers to proceed in the S_0

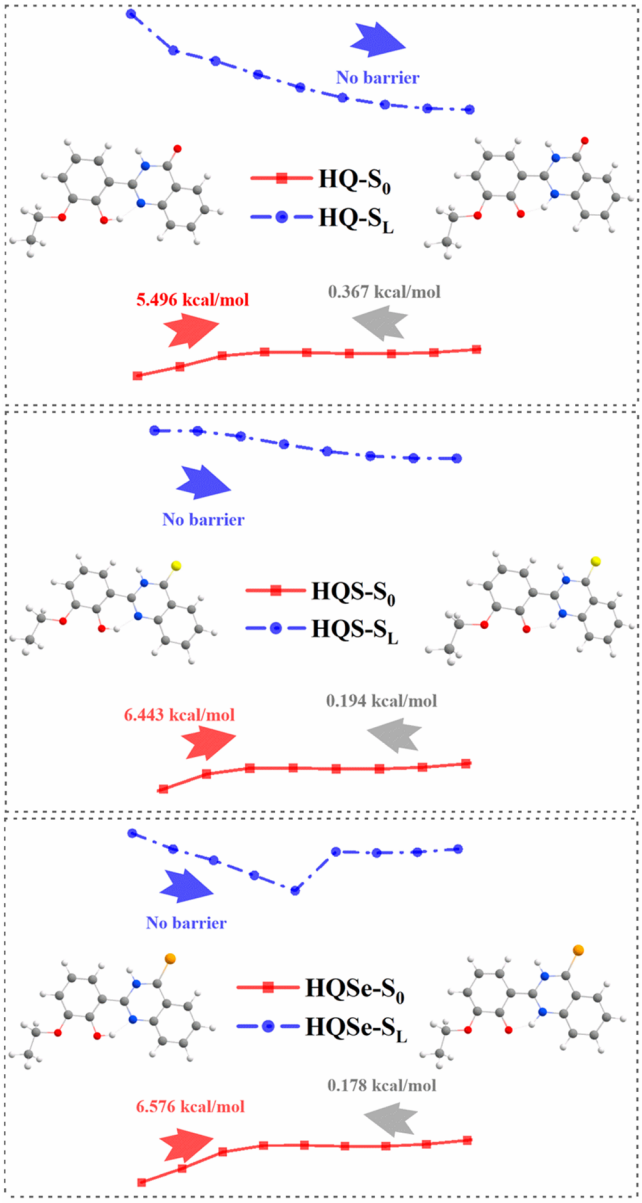

Figure 6. Potential energy curves of HQ, HQS, and HQSe in S_0 and S_L states along with the growing trend of O_1−H_1 bond length.

https://doi.org/10.1021/acsomega.2c00316
ACS Omega 2022, 7, 14848−14855

state, which is in agreement with the relative stronger $O_1\cdots H_1-N_1$ IHB in the S_0 state.

In addition, it can be found that the energy barriers of reverse ground-state intramolecular proton transfer (RGSIPT) of HQ, HQS, and HQSe are far lower than the energy barriers of ground-state intramolecular proton transfer (GSIPT) and ESIPT.[60−62] Thus, it can be found that the three compounds can quickly return to the enol form in the S_0 state, and it is favorable to enhance the effective acting time of sunscreen.

4. CONCLUSION

In this work, the effects of atomic substitution on the ESIPT process of HQ have been comprehensively investigated by DFT and TD-DFT methods. From calculated results, it can be found that the IHBs of HQ, HQS, and HQSe are weakened in the S_L state, indicating that it is difficult for RPT to occur in the S_L states. The absorption and fluorescence peaks of HQS and HQSe are separately located in the range of UVA and visible light, which corresponds to sunscreen requirements, and it can be found that the quantity of transferred electrons can affect the strength of fluorescence peaks of molecules. Moreover, as a result of the analysis of the PECs, it can be concluded that HQ, HQS, and HQSe are not energy barrier processes, which is favorable for ESIPT to occur. Moreover, the energy barriers of RGSIPT of HQ, HQS, and HQSe are lower than the energy barriers of GSIPT, indicating the three compounds can quickly go back to the enol form at the ground state, and it is favorable to enhance the effective acting time of sunscreen. All in all, this provides a theoretical foundation for synthesizing the new compounds applied to sunscreen.

■ ASSOCIATED CONTENT

Supporting Information

The Supporting Information is available free of charge at https://pubs.acs.org/doi/10.1021/acsomega.2c00316.

Figure S1 (PDF)

■ AUTHOR INFORMATION

Corresponding Author

Chaofan Sun − *College of Science, Northeast Forestry University, Harbin, Heilongjiang 150040, China;* orcid.org/0000-0002-1273-6707; Email: cfsun@nefu.edu.cn

Authors

Yajie Zhang − *College of Science, Northeast Forestry University, Harbin, Heilongjiang 150040, China*

Min Ma − *College of Science, Northeast Forestry University, Harbin, Heilongjiang 150040, China*

Changjiao Shang − *College of Science, Northeast Forestry University, Harbin, Heilongjiang 150040, China*

Yunjian Cao − *College of Science, Northeast Forestry University, Harbin, Heilongjiang 150040, China*

Complete contact information is available at: https://pubs.acs.org/10.1021/acsomega.2c00316

Notes

The authors declare no competing financial interest.

■ ACKNOWLEDGMENTS

This work was supported by the Fundamental Research Funds for the Central Universities (2572020BC03).

■ REFERENCES

(1) Armstrong, B. K.; Kricker, A. The epidemiology of UV induced skin cancer. *Photobiol. B* **2001**, *63* (1−3), 8−18.

(2) Martincorena, I.; Roshan, A.; Gerstung, M.; Ellis, P.; Van Loo, P.; McLaren, S.; Wedge, D. C.; Fullam, A.; Alexandrov, L. B.; Tubio, J. M.; et al. High burden and pervasive positive selection of somatic mutations in normal human skin. *Science* **2015**, *348* (6237), 880−886.

(3) Krauthammer, M.; Kong, Y.; Ha, B. H.; Evans, P.; Bacchiocchi, A.; McCusker, J. P.; Cheng, E.; Davis, M. J.; Goh, G.; Choi, M.; et al. Exome sequencing identifies recurrent somatic RAC1 mutations in melanoma. *Nat. Genet.* **2012**, *44* (9), 1006.

(4) Thompson, A. J.; Hart-Cooper, W. M.; Cunniffe, J.; Johnson, K.; Orts, W. J. Safer Sunscreens: Investigation of Naturally Derived UV Absorbers for Potential Use in Consumer Products. *ACS Sustainable Chem. Eng.* **2021**, *9* (27), 9085−9092.

(5) Kao, M.-H.; Venkatraman, R. K.; Sneha, M.; Wilton, M.; Orr-Ewing, A. J. Influence of the Solvent Environment on the Ultrafast Relaxation Pathways of a Sunscreen Molecule Diethylamino Hydroxybenzoyl Hexyl Benzoate. *J. Phys. Chem. A* **2021**, *125* (2), 636−645.

(6) Muramatsu, S.; Nakayama, S.; Kinoshita, S.-n.; Onitsuka, Y.; Kohguchi, H.; Inokuchi, Y.; Zhu, C.; Ebata, T. Electronic State and Photophysics of 2-Ethylhexyl-4-methoxycinnamate as UV-B Sunscreen under Jet-Cooled Condition. *J. Phys. Chem. A* **2020**, *124* (7), 1272−1278.

(7) Giokas, D. L.; Salvador, A.; Chisvert, A. UV filters: From sunscreens to human body and the environment. *TrAC, Trends Anal. Chem.* **2007**, *26* (5), 360−374.

(8) Silvia Diaz-Cruz, M.; Llorca, M.; Barcelo, D.; Barcelo, D. Organic UV filters and their photodegradates, metabolites and disinfection by-products in the aquatic environment. *TrAC, Trends Anal. Chem.* **2008**, *27* (10), 873−887.

(9) Kurz, W.; Yetisen, A. K.; Kaito, M. V.; Fuchter, M. J.; Jakobi, M.; Elsner, M.; Koch, A. W. UV-Sensitive Wearable Devices for Colorimetric Monitoring of UV Exposure. *Adv. Opt. Mater.* **2020**, *8* (6), 1901969.

(10) Paterson, M. J.; Robb, M. A.; Blancafort, L.; DeBellis, A. D. Theoretical study of benzotriazole UV photostability: Ultrafast deactivation through coupled proton and electron transfer triggered by a charge-transfer state. *J. Am. Chem. Soc.* **2004**, *126* (9), 2912−2922.

(11) Zhou, P. W.; Han, K. Unraveling the Detailed Mechanism of Excited-State Proton Transfer. *Acc. Chem. Res.* **2018**, *51* (7), 1681−1690.

(12) Li, C. X.; Guo, W. W.; Xie, B. B.; Cui, G. L. Photodynamics of oxybenzone sunscreen: Nonadiabatic dynamics simulations. *J. Chem. Phys.* **2016**, *145* (7), 074308.

(13) Sun, C. F.; Su, X.; Zhou, Q.; Shi, Y. Regular tuning of the ESIPT reaction of 3-hydroxychromone-based derivatives by substitution of functional groups. *Org. Chem. Front.* **2019**, *6* (17), 3093−3100.

(14) Yin, H.; Li, H.; Xia, G. M.; Ruan, C. Y.; Shi, Y.; Wang, H. M.; Jin, M. X.; Ding, D. J. A novel non-fluorescent excited state intramolecular proton transfer phenomenon induced by intramolecular hydrogen bonds: an experimental and theoretical investigation. *Sci. Rep.* **2016**, *6*, 19774.

(15) Kwon, J. E.; Park, S. Y. Advanced Organic Optoelectronic Materials: Harnessing Excited-State Intramolecular Proton Transfer (ESIPT) Process. *Adv. Mater.* **2011**, *23* (32), 3615−3642.

(16) Padalkar, V. S.; Seki, S. Excited-state intramolecular proton-transfer (ESIPT)-inspired solid state emitters. *Chem. Soc. Rev.* **2016**, *45* (1), 169−202.

(17) He, L. W.; Dong, B. L.; Liu, Y.; Lin, W. Y. Fluorescent chemosensors manipulated by dual/triple interplaying sensing mechanisms. *Chem. Soc. Rev.* **2016**, *45* (23), 6449−6461.

(18) Wu, Z.; Wang, M.; Guo, Y.; Ji, F.; Wang, C.; Wang, S.; Zhang, J.; Wang, Y.; Zhang, S.; Jin, B.; et al. Nonadiabatic Dynamics Mechanism of Chalcone Analogue Sunscreen FPPO-HBr: Excited

State Intramolecular Proton Transfer Followed by Conformation Twisting. *J. Phys. Chem. B* **2021**, *125* (33), 9572−9578.
(19) Holt, E. L.; Krokidi, K. M.; Turner, M. A. P.; Mishra, P.; Zwier, T. S.; Rodrigues, N. D. N.; Stavros, V. G. Insights into the photoprotection mechanism of the UV filter homosalate. *Chem. Chem. Phys.* **2020**, *22* (27), 15509−15519.
(20) Ji, F. X.; Guo, Y. R.; Wang, M. Q.; Wang, C.; Wu, Z. B.; Wang, S. P.; Wang, H. Y.; Feng, X.; Zhao, G. J. New insights into ESIPT mechanism of three sunscreen compounds in solution: A combined experimental and theoretical study. *Colloids Surf., B* **2021**, *207*, 112039.
(21) Moshkina, T. N.; Nosova, E. V.; Lipunova, G. N.; Valova, M. S.; Petrusevich, E. F.; Zalesny, R.; Osmialowski, B.; Charushin, V. N. Substituted 2-(2-hydroxyphenyl)-3H-quinazolin-4-ones and their difluoroboron complexes: Synthesis and photophysical properties. *Spectrochim. Acta, Part A* **2021**, *252*, 119497.
(22) Hohenberg, P.; Kohn, W. Inhomogeneous electron gas. *Phys. Rev.* **1964**, *136* (3B), B864−B871.
(23) Kohn, W.; Sham, L. J. Quantum density oscillations in an inhomogeneous electron gas. *Phys. Rev.* **1965**, *137* (6A), A1697−A1705.
(24) Liu, S.; Zhao, X.; Li, Y.; Chen, M.; Sun, M. DFT study of adsorption site effect on surface-enhanced Raman scattering of neutral and charged pyridine−Ag4 complexes. *Spectrochim. Acta, Part A* **2009**, *73* (2), 382−387.
(25) Stratmann, R. E.; Scuseria, G. E.; Frisch, M. J. An efficient implementation of time-dependent density-functional theory for the calculation of excitation energies of large molecules. *J. Chem. Phys.* **1998**, *109* (19), 8218−8224.
(26) Matsuzawa, N. N.; Ishitani, A.; Dixon, D. A.; Uda, T. Time-dependent density functional theory calculations of photoabsorption spectra in the vacuum ultraviolet region. *J. Phys. Chem. A* **2001**, *105* (20), 4953−4962.
(27) Li, Q. J.; Ding, Q. Q.; Lin, W. H.; Wang, J. C.; Chen, M. D.; Sun, M. T. Surface-enhanced Raman scattering of pyrazine on Au5Al5 bimetallic nanoclusters. *RSC Adv.* **2017**, *7* (20), 12170−12178.
(28) Lee, C.; Yang, W.; Parr, R. G. Development of the Colle-Salvetti correlation-energy formula into a functional of the electron density. *Phys. Rev. B* **1988**, *37* (2), 785−789.
(29) Becke, A. D. Density-functional exchange-energy approximation with correct asymptotic behavior. *Phys. Rev. A* **1988**, *38* (6), 3098−3100.
(30) Becke, A. D. Densityâ functional thermochemistry. I. The effect of the exchangeâ only gradient correction. *J. Chem. Phys.* **1992**, *96* (3), 2155−2160.
(31) Lou, Z.; Zhou, X.; Tang, Z.; Zhou, P. Theoretical Insights into the Excited State Decays of a Donor−Acceptor Dyad: Is the Twisted and Rehybridized Intramolecular Charge-Transfer State Involved? *J. Phys. Chem. B* **2020**, *124* (22), 4564−4572.
(32) Cossi, M.; Scalmani, G.; Rega, N.; Barone, V. New developments in the polarizable continuum model for quantum mechanical and classical calculations on molecules in solution. *J. Chem. Phys.* **2002**, *117* (1), 43−54.
(33) Scalmani, G.; Frisch, M. J. Continuous surface charge polarizable continuum models of solvation. I. General formalism. *J. Chem. Phys.* **2010**, *132* (11), 114110.
(34) Lu, T.; Chen, F. W. Multiwfn: A multifunctional wavefunction analyzer. *J. Comput. Chem.* **2012**, *33* (5), 580−592.
(35) Humphrey, W.; Dalke, A.; Schulten, K. VMD: visual molecular dynamics. *J. Mol. Graphics* **1996**, *14* (1), 27−38.
(36) Frisch, M. J.; et al. *Gaussian 16*, revision C.01; Gaussian Inc.: Wallingford, CT, 2016.
(37) Yu, Y.; Chu, B.; Tang, Z.; He, H.; Zhou, P. Blocking the dark state as sensing mechanism of 3-nitro-1,8-naphthalimide derivatives for detection of carbon monoxide in the living cells. *Dyes Pigm.* **2022**, *197*, 109905.
(38) Shang, C. J.; Cao, Y. J.; Sun, C. F.; Li, Y. Z. Tuning fluorescence behavior and ESIPT reaction of 2-(2-Hydroxy-phenyl)-4(3H)-quinazolinone by introducing different groups. *J. Lumin.* **2021**, *235*, 118059.
(39) Cao, Y. J.; Wang, L. L.; Liu, Z. Q.; Sun, C. F.; Li, Y. Z. Theoretical study on the sensing mechanism of chalcone-based fluorescence probe for detecting hydrogen sulfide and biothiols. *New J. Chem.* **2021**, *45* (36), 16906−16912.
(40) Zhao, J.; Li, Z.; Jin, B. Uncovering photo-induced hydrogen bonding interaction and proton transfer mechanism for the novel salicylaldehyde azine derivative with para-position electrophilic cyano group. *J. Lumin.* **2021**, *238*, 118231.
(41) Das, R.; Bej, S.; Hirani, H.; Banerjee, P. Trace-Level Humidity Sensing from Commercial Organic Solvents and Food Products by an AIE/ESIPT-Triggered Piezochromic Luminogen and ppb-Level "OFF-ON-OFF" Sensing of Cu2+: A Combined Experimental and Theoretical Outcome. *ACS Omega* **2021**, *6* (22), 14104−14121.
(42) Cao, B. F.; Li, Y.; Zhou, Q.; Li, B.; Su, X.; Yin, H.; Shi, Y. Synergistically improving myricetin ESIPT and antioxidant activity via dexterously trimming atomic electronegativity. *J. Mol. Liq.* **2021**, *325*, 115272.
(43) Qi, Y.; Tang, Z.; Zhan, H.; Wang, Y.; Zhao, Y.; Fei, X.; Tian, J.; Yu, L.; Liu, J. A new interpretation of the ESIPT mechanism of 2-(benzimidazol-2-yl)-3-hydroxychromone derivatives. *Spectrochim. Acta, Part A* **2020**, *224*, 117359.
(44) Zhao, G.; Yang, Y.; Zhang, C.; Song, Y.; Li, Y. The theoretical study of excited-state intramolecular proton transfer of N, N,-bis (salicylidene)-(2-(3″4●-diaminophenyl) benzothiazole). *J. Lumin.* **2021**, *230*, 117741.
(45) Zhao, G.; Shi, W.; Yang, Y.; Ding, Y.; Li, Y. Substituent Effects on Excited-State Intramolecular Proton Transfer Reaction of 2-Aryloxazoline Derivatives. *J. Phys. Chem. A* **2021**, *125* (13), 2743−2750.
(46) Yang, Y. F.; Zhao, J. F.; Li, Y. Q. Theoretical Study of the ESIPT Process for a New Natural Product Quercetin. *Sci. Rep.* **2016**, *6*, 32152.
(47) Lu, T.; Chen, Q. Interaction Region Indicator: A Simple Real Space Function Clearly Revealing Both Chemical Bonds and Weak Interactions. *Chem. Methods* **2021**, *1* (5), 231−239.
(48) Liang, X. N.; Fang, H. Fine-tuning directionality of ESIPT behavior of the asymmetric two proton acceptor system via atomic electronegativity. *Spectrochim. Acta, Part A* **2022**, *266*, 120406.
(49) Liu, S. S.; Zhao, Y.; Zhang, C. Z.; Lin, L. L.; Li, Y. Q.; Song, Y. Z. The novel excited state intramolecular proton transfer broken by intermolecular hydrogen bonds in HOF system. *Spectrochim. Acta, Part A* **2019**, *219*, 164−172.
(50) Ding, S.; Xu, A. X.; Sun, A. K.; Xia, Y.; Liu, Y. J. An Excited State Intramolecular Proton Transfer-Based Fluorescent Probe with a Large Stokes Shift for the Turn-on Detection of Cysteine: A Detailed Theoretical Exploration. *ACS Omega* **2020**, *5* (31), 19695−19701.
(51) Zhou, P. W.; Ning, C.; Alsaedi, A.; Han, K. L. The Effects of Heteroatoms Si and S on Tuning the Optical Properties of Rhodamine- and Fluorescein-Based Fluorescence Probes: A Theoretical Analysis. *ChemPhysChem* **2016**, *17* (19), 3139−3145.
(52) Sinha, S.; Chowdhury, B.; Ghosh, P. A Highly Sensitive ESIPT-Based Ratiometric Fluorescence Sensor for Selective Detection of Al3+. *Inorg. Chem.* **2016**, *55* (18), 9212−9220.
(53) Liu, Z. Y.; Lu, T.; Chen, Q. X. An sp-hybridized all-carboatomic ring, cyclo 18 carbon: Electronic structure, electronic spectrum, and optical nonlinearity. *Carbon* **2020**, *165*, 461−467.
(54) Brito da Silva, C.; Gil, E. S.; da Silveira Santos, F.; Moras, A. M.; Steffens, L.; Bruno Goncalves, P. F.; Moura, D. J.; Ludtke, D. S.; Rodembusch, F. S. Proton-Transfer-Based Azides with Fluorescence Off-On Response for Detection of Hydrogen Sulfide: An Experimental, Theoretical, and Bioimaging Study. *J. Org. Chem.* **2018**, *83* (24), 15210−15224.
(55) Yang, Y.; Luo, X.; Ma, F.; Li, Y. Substituent effect on ESIPT mechanisms and photophysical properties of HBT derivatives. *Spectrochim. Acta, Part A* **2021**, *250*, 119375.
(56) Zhao, J.; Jin, B. Solvent polarity dependent excited state hydrogen bond effects and intramolecular double proton transfer

https://doi.org/10.1021/acsomega.2c00316
ACS Omega 2022, 7, 14848−14855

mechanism for 2-hydroxyphenyl-substituted benzo[1,2-d:4,5-d']-bisimidazole system. *Spectrochim. Acta, Part A* **2021**, *250*, 119394.
(57) Sun, C. F.; Zhang, X.; Diao, L. H.; Cao, B. F.; Yin, H.; Shi, Y. How the atomic electron -accepting ability affect the double ESIPT process of 2,5-bis(benzoxazol-2-yl)thiophene-3,4-diol? *J. Lumin.* **2020**, *225*, 117329.
(58) Coelho, F. L.; da Costa Duarte, R.; de Avila Braga, C.; Toldo, J. M.; Bruno Goncalves, P. F.; da Silveira Santos, F.; Rodembusch, F. S. Benzothiazole merocyanine dyes as middle pH optical sensors. *Dyes Pigm.* **2020**, *176*, 108193.
(59) Kanlayakan, N.; Kungwan, N. Theoretical study of heteroatom and substituent effects on excited-state intramolecular proton transfers and electronic properties of amino-type hydrogen bonding molecules. *J. Lumin.* **2021**, *238*, 118260.
(60) Tang, J.; Robichaux, M. A.; Wu, K. L.; Pei, J. Q.; Nguyen, N. T.; Zhou, Y. B.; Wensel, T. G.; Xiao, H. Single-Atom Fluorescence Switch: A General Approach toward Visible-Light-Activated Dyes for Biological Imaging. *J. Am. Chem. Soc.* **2019**, *141* (37), 14699−14706.
(61) Tang, Z.; Li, P.; Liu, J.; Zhou, P. Carbonyl Stretch as a Franck−Condon Active Mode and Driving Force for Excited-State Decay of 8-Methoxy-4-methyl-2H-benzo[g]chromen-2-one from nπ^* State. *J. Phys. Chem. B* **2020**, *124* (50), 11472−11480.
(62) Zhou, P.; Tang, Z.; Li, P.; Liu, J. Unraveling the Mechanism for Tuning the Fluorescence of Fluorescein Derivatives: The Role of the Conical Intersection and nπ^* State. *J. Phys. Chem. Lett.* **2021**, *12* (28), 6478−6485.

https://doi.org/10.1021/acsomega.2c00316
ACS Omega 2022, 7, 14848−14855